CrossMark

Optimizing of Gold Nanoparticles on Porous Silicon Morphologies for a Sensitive Carbon Monoxide Gas Sensor Device

Amer B. Dheyab[1] · Alwan M. Alwan[2] · Mehdi Q. Zayer[2]

Abstract

A set of carbon monoxide (CO) gas sensors based on porous silicon (PSi)/gold nanoparticle (AuNP) hetro structures were fabricated. *Different* forms of PSi surface morphologies were studied as a substrate for growth of AuNPs. Simple dipping process of PSi in hydrogen tetrachloroaurate (III) solution (HAuCl$_4$) at fixed concentrations of 10^{-2} M/3.5 HF was used to synthesize AuNPs. The n-type PSi was equipped through photo-electrochemical etching process at current density value of 10 mA/cm^2 under illumination condition of 530-nm wavelength and laser illumination intensity of 20 to 80 mW/cm^2. Three different forms of PSi morphology, meso, macro, and double layers with pore shapes and sizes, were prepared. The structural and surface morphology properties of PSi-based substrate before and after deposition of AuNPs were investigated through studying of scanning electron microscopy (SEM), photoluminescence (PL), and X-ray diffraction (XRD). The electrical property (J-V) was carried out in primary vacuum and CO at low pressure. The results show that PSi surface morphologies strongly influenced the AuNP sizes and hence the sensor performance. It was found that decrease the AuNP sizes could be occasioned in high and fast current response.

Keywords PSi · SEM · Response · Recovery · AuNP hetro structures · Gas sensing

Introduction

Porous silicon (PSi) has attracted much attention as a promising electronic material since as a result of its outstanding mechanical and thermal features and its low charge [1–3]. The high surface area inside a slight volume, its well-regulated morphologies, and its high chemical activity make it to be remarkable candidate for gas sensing applications [4, 5]. Gas sensors on the market today have many limitations that prevent real-world applications. The largest issues with current sensors are that the sensors cannot differentiate between gasses and also struggle to detect gasses at low concentrations. PSi is optimal for gas sensing because it operates at room temperature, has a large surface area, can be created with a hybrid micro/nanostructure for sensitivity, and can be produced using well-known etching techniques. The surface morphology of the silicon skeleton, the pore shape, and the density of the dangling bonds can be influenced by many etching parameters especially the etching current density and laser illumination power densities [6, 7]. Modifying the surface morphologies of porous layer by incorporating metallic nanoparticles represents as procedures for improving the performance of gas sensors owing to its catalytic property [8–11]. In this work, Al/PSi/AuNP n-Si/Al hetro structure has been fabricated and tested as carbon monoxide gas sensors operated at room temperature. The role of porous silicon morphologies on growth and morphology of gold nanoparticle (AuNP) that improves the performance of the hetro sensors has been examined. The surface morphologies of PSi layer before and after incorporation of AuNPs were studied by SEM, EDS, J-V, and XRD analysis.

✉ Amer B. Dheyab
amer.aljoburi@yahoo.com

1 Ministry of Science and Technology, Baghdad, Iraq

2 School of Applied Science, University of Technology, Baghdad, Iraq

Experimental Details

PSi substrates were fabricate via photo-electrochemical etching of (100) n-type silicon wafer of resistivity 100 Ω cm in a
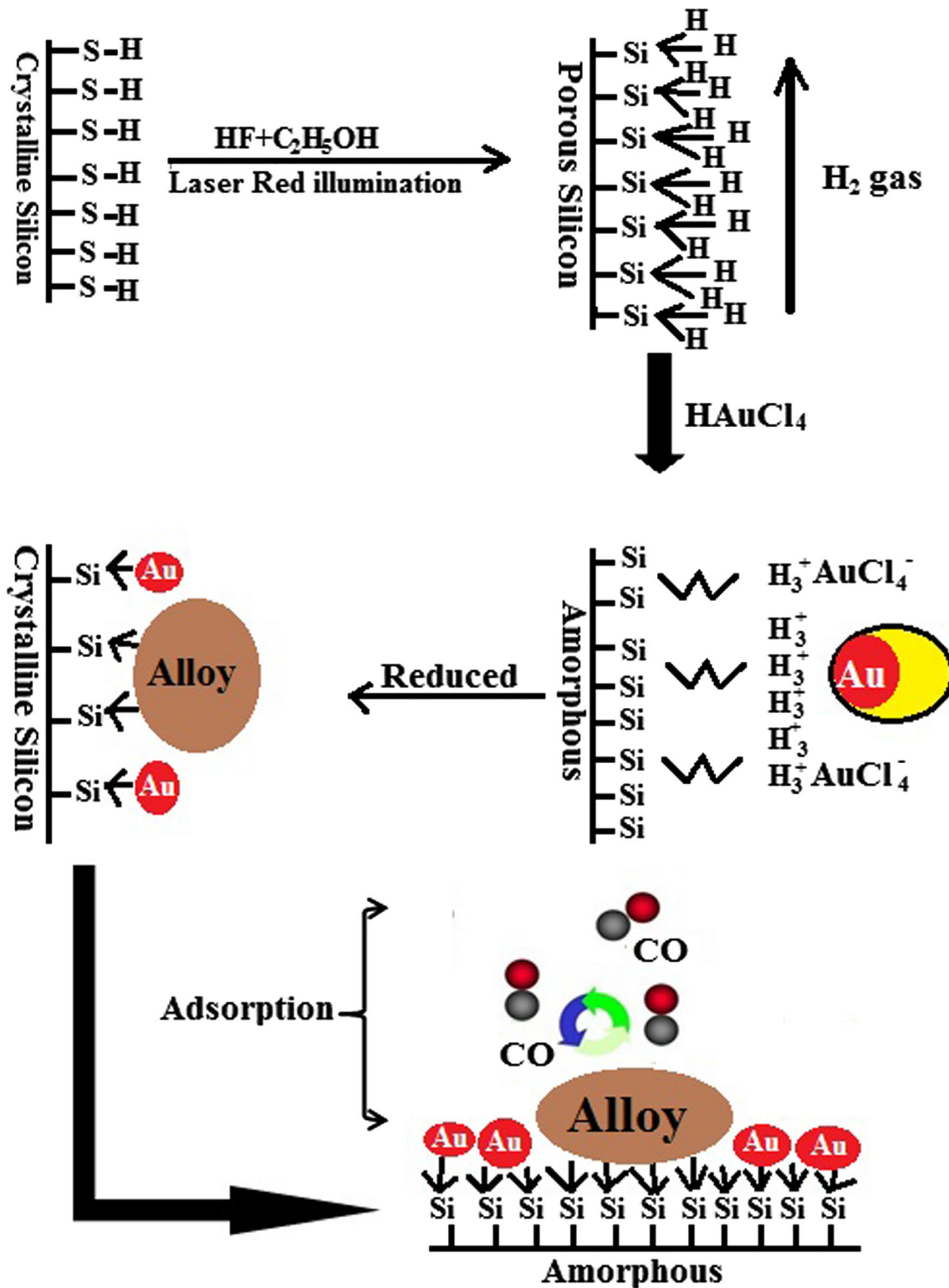
Fig. 1 Schematic illustration of the procedures for synthesis of AuNP/PSi hetro structures

2:1 HF(48%):C_2H_5OH (99%) solution at current density of 10 mA/cm^2 under illumination condition of 530-nm wavelength and laser illumination power density of 20 to 80 mW/cm^2, in a Teflon single etching cell.

Fig. 2 a, **b** The dependence of porosity and depth as a function to laser power density
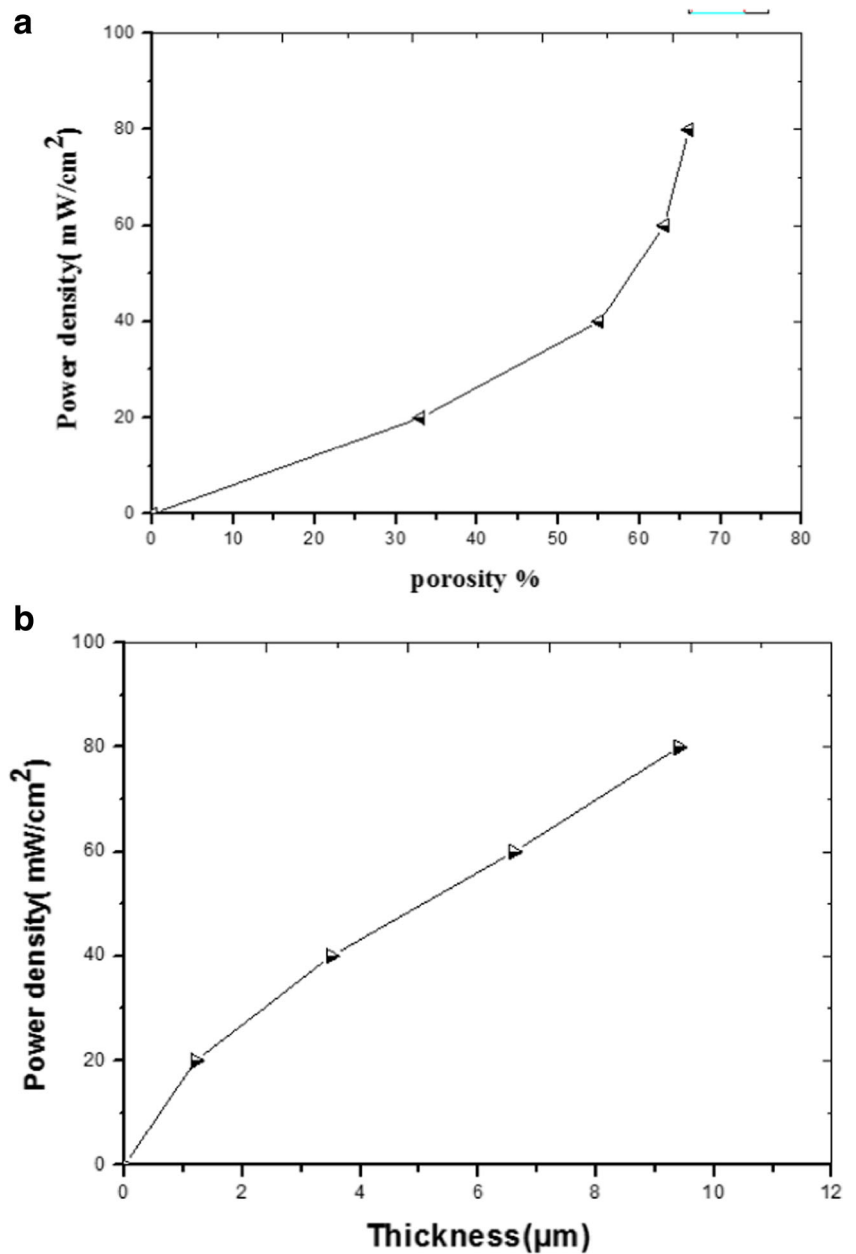
The silicon substrates have been washed using high-purity 99.9% ethanol. The silicon substrate acts as the anode, while the cathode was a ring of platinum electrode (Pt) and dipped in 20% hydrofluoric acid (HF) concentration.

After formation, the PSi substrates were cleaned in distilled water and allowed to dry with nitrogen stream. AuNPs were incorporated on PSi layers by ion reduction process after immersing the interface into aqueous solutions of $HAuCl_4$/HF with 10^{-2} M/3.5 HF for 5 min at room temperature as in Fig. 1. The growth of AuNPs occurs by means of the reduction of metal ion via

dangling bonds of the PSi layer as shown in the following reaction [8]:

$$Si + 6HF \rightarrow H_2SiF_6 + 4H^+ 4e \qquad (1)$$

$$Au^{3+} + 3e^- \rightarrow Au \qquad (2)$$
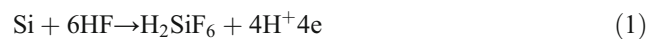
The subsequent AuNP/PSi hetro structures were lastly rinsed with deionized water and dried with N_2 gas. The electrical contact over the AuNP/PSi layer was fabricated by depositing a thin aluminum layer.
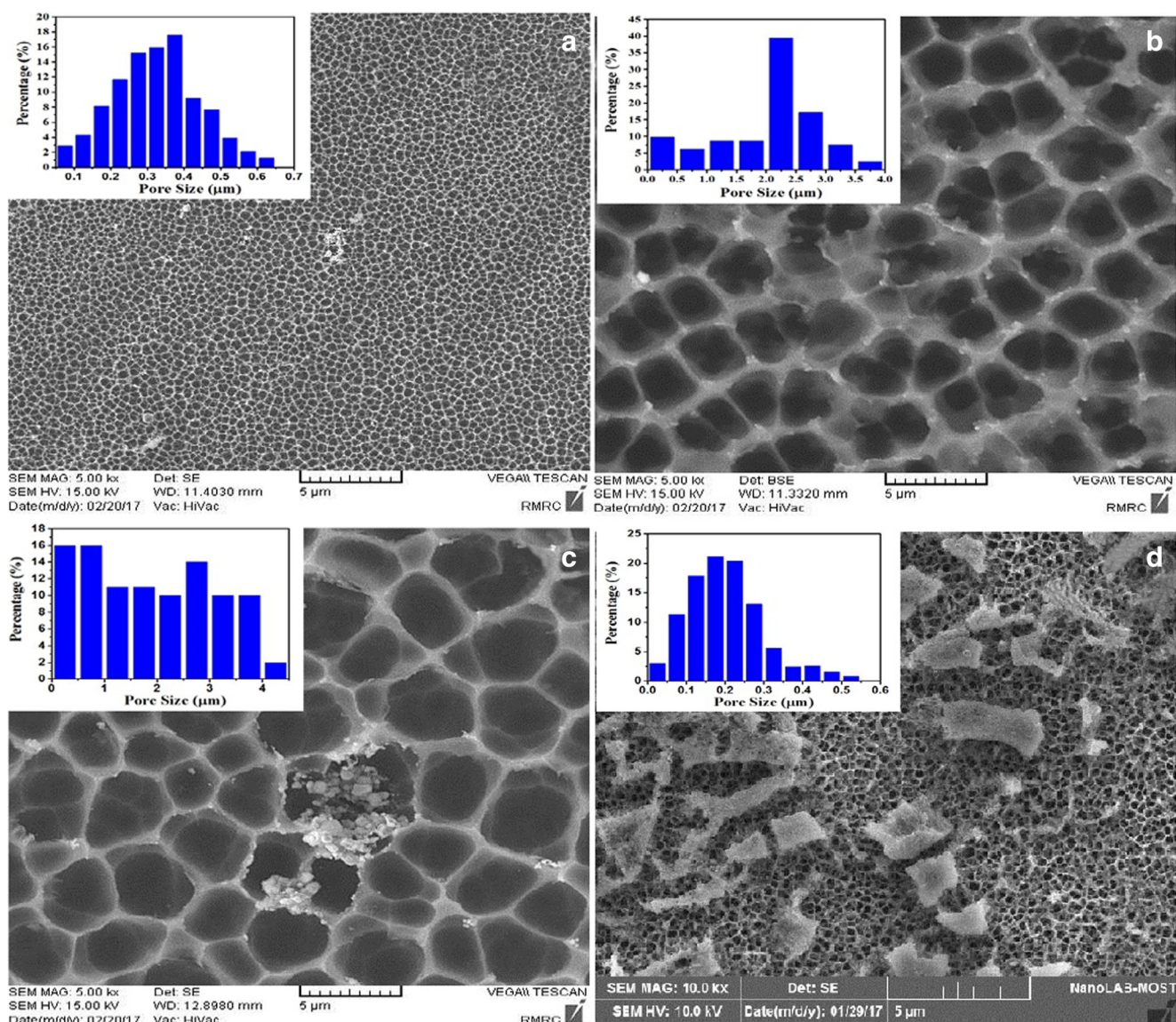
Fig. 3 SEM images of porous silicon and statically pore diameter distributions as a function to laser power density: (a) 20 mW/cm^2, (b) 40 mW/cm^2, (c) 60 mW/cm^2, and (d) 80 mW/cm^2

After the formation of AuNP/PSi hetro structures, a thin aluminum layer of about 10 nm was deposited on the AuNPs by high vacuum pressure with base pressure of about 2×10^{-4}. Another aluminum electrode was deposited on the lower silicon surface in such a way that the electrical current is carried out perpendicular to PSi hetro structures. The sensors were tested at fixed CO gas pressure of about 2 mbar in a sealed cavity with inlet and outlet points.

Results and Discussion

Structural Properties of As-Formed PSi

Figure 2a, b shows the variation of porosity and depth as a function to laser power density. The porosity and layer depth of PSi substrate was calculated based on gravimetric method [9].

As shown in Fig. 2a, the porosity grows exponentially with increasing illumination power density. Porosity of the PSi starts from 31% at laser power density of 20 mW/cm^2 and exceeds 64% at high power density of 80 mW/cm^2. Figure 2b shows the correlation between depth of PSi layer and laser power density ranging from 20 to 80 mW/cm^2, where the depth of PSi layer growing with laser power density and the depth varies from 1 to about 9.2 μm. This growth in both porosity and layer depth is because of the rise of Si disbanding process that happens as a result of the growing photo created electron—hole pairs caused by photon absorption process [9].

Figure 3(a–d) presents the surface morphology of the resulting meso and macro PSi layer prepared at different laser
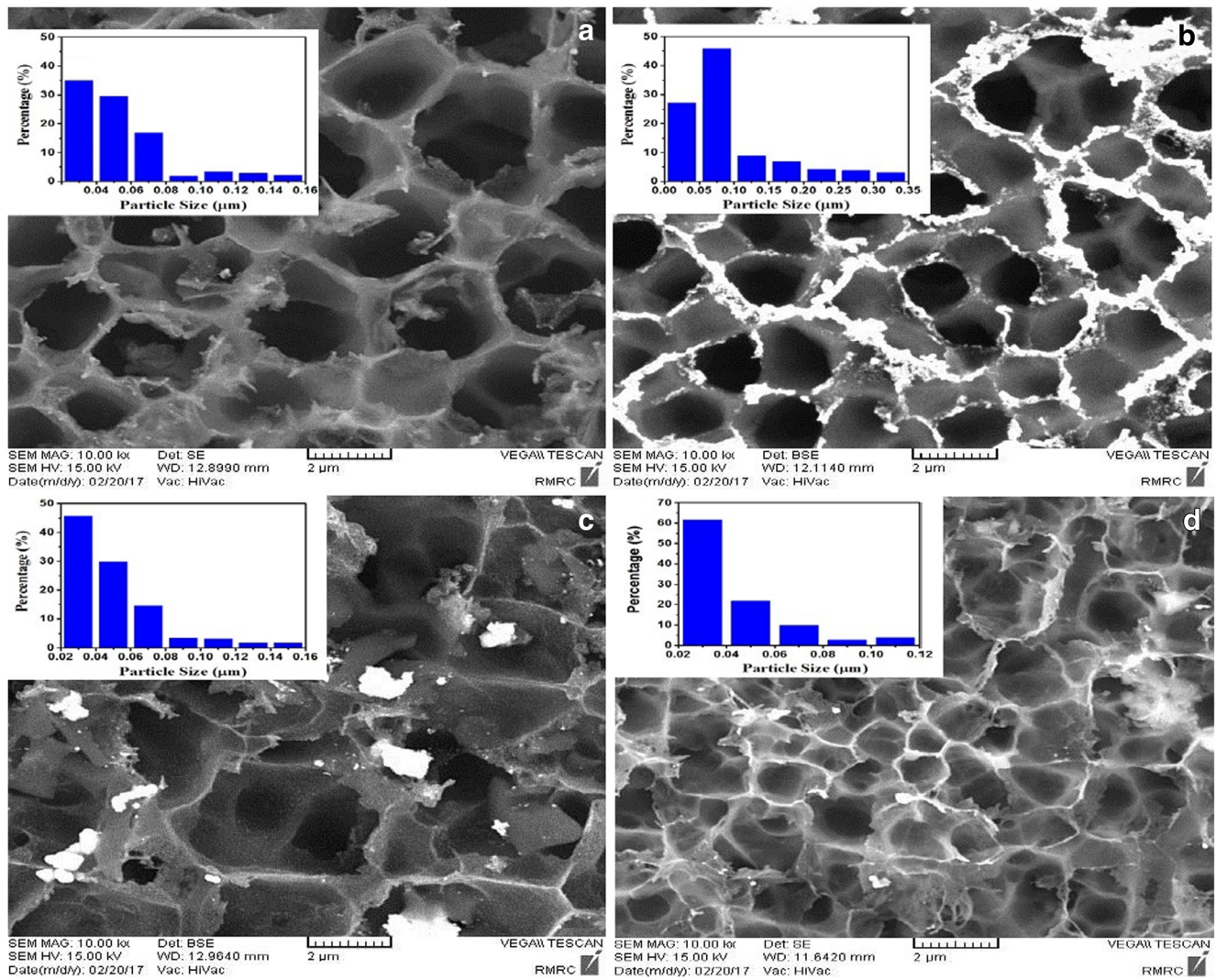
Fig. 4 SEM images of AuNP/PSi hetro structures with the statically AuNP size distributions as a function to laser power density: (a) 20 mW/cm^2, (b) 40 mW/cm^2, (c) 60 mW/cm^2, and (d) 80 mW/cm^2

power densities. Three different forms of PSi morphologies; meso, macro, and double layers with pore shapes and sizes were prepared. These were employed to synthesis of AuNPs. Surface morphology looks like a pore-like structure, and the pores have different shapes which arbitrarily spread, perpendicularly on PSi surface. An increase in pore size and combination process of adjacent pores lead to modifying it from circular to randomly shaped pores. Meso PSi layer was observed at lower illumination power density of 20 mW/cm^2 Fig. 3(a); the pores size distribution was varied (0.075 to 0.625 μm) and the highest value of the histogram was at 0.375 μm. Figure 3(b, c) illustrates that the formation of macro PSi layer with size distribution of pores varied from 0.25 to 3.75 μm and from 0.25 to 4.25 μm at illumination power densities of 40 mW/cm^2 and 60 mW/cm^2 respectively. Double PSi layer as presented in Fig. 4(d) was formed at higher illumination power density of about 80 mW/cm^2, and the pore size distribution was varied from 0.025 to 0.525 μm,

this range extending both on meso PSi and macro PSi layers. The existence of double PSi layer and the transition of morphology take place simultaneously due to the high etching rates which occur when laser generation of electron hole pairs exceeds the recombination rates especially at high laser power [9–11].

Structural Properties of AuNP/PSi Hetro Structures

The surface nature of the deposited AuNPs as a function of porous morphology over the PSi layer is illustrated in Fig. 4(a–d). The aggregated AuNPs are mainly located on the pore walls with different sizes and forms. In Fig. 4(a), the sizes of AuNPs fluctuate from 30 to 150 nm, and the higher value of distribution is about 30 nm; while in Fig. 4(b), the AuNPs fluctuate from 25 to 325 nm, and the peak distribution is about 75 nm. In Fig. 4(c), size fluctuates from 30 to 150 nm, and the higher value of distribution is
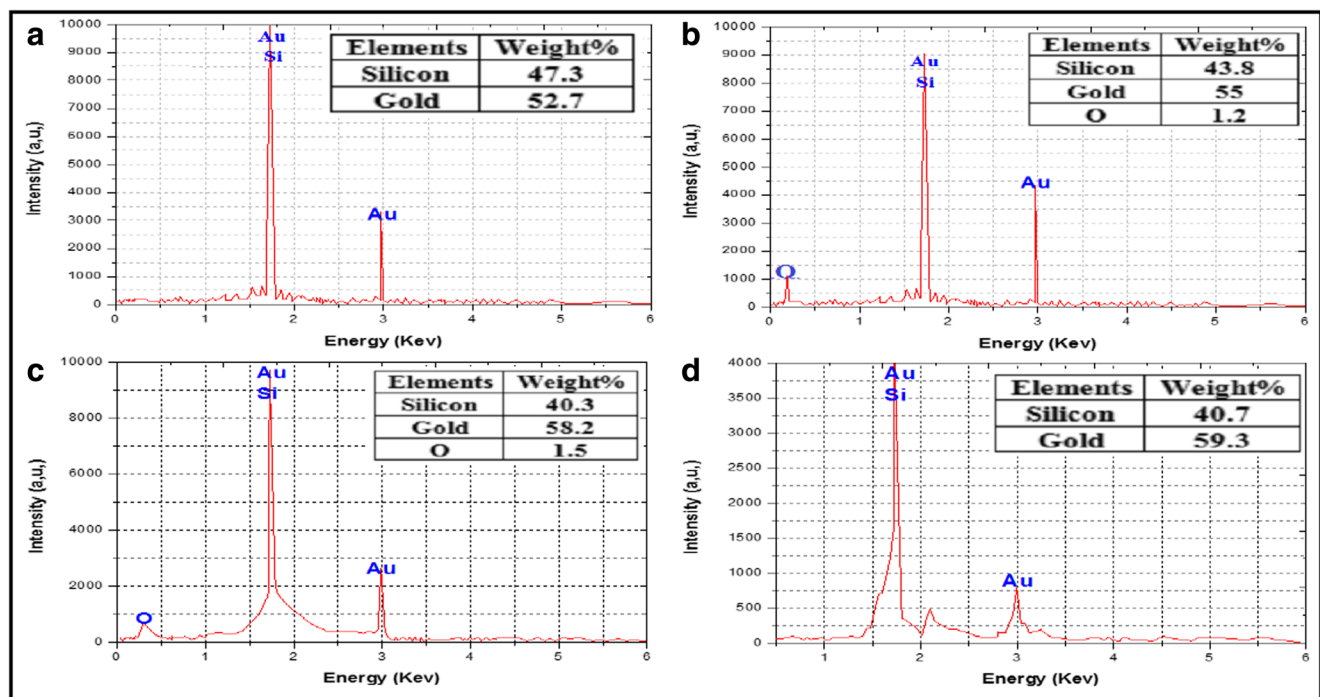
Fig. 5 EDX spectra of AuNPs deposited over PSi layer as a function to laser power density: (a) 20 mW/cm^2, (b) 40 mW/cm^2, (c) 60 mW/cm^2, and (d) 80 mW/cm^2

about 30 nm. Finally, in Fig. 4(d), the AuNPs fluctuate from 30 to 110 nm, and the higher value of distribution is about 20 nm. Minimum AuNP size was obtained with double PSi layer due to the density of nucleation sites [10].

EDX spectra of AuNPs deposited over PSi layer are shown in Fig. 5. The EDS analysis confirms the existence and the amount of AuNPs over the PSi layer. The weight ratio is about 52.7, 55, 58.2, and 59.3% for deposition solution 10^{-2} M/2.8 HF. Higher density of AuNPs was recorded at PSi layer of higher porosity with double morphology behavior as a result of high density of dangling bond (AuNPs) nucleation sites.

The X-ray diffraction spectra of AuNPs, fabricated by photo electrochemical etching as a function to laser power density, are displayed in Fig. 6. Malty diffraction peaks at 38.2°, 44.4°, and 64.6° which represent (100), (200), and (220) planes of pure gold (ASTM Standard Card). It approves that gold is the chief composition of the nanoparticles (Table 1).

Here we see the reliance of AuNP sizes and their specific surface area on the laser power density is new features for controlling the properties of AuNPs. The width of diffraction peak is depended by the crystallite sizes. The broadness of the XRD peak gives an indication of the crystalline size distribution. Big AuNP crystallite sizes affect sharp reflections, while slight size affects principally wider reflections [9]. Table 2 displays an incessant rise in the grain size of the AuNPs in the planes (111) and (200) of AuNP/PSi hetro structures when growing the laser power density. In contrast, grain size is lessening in the plane (111).

The smallest AuNP grain size is around 1.9 nm at 80 mW/cm^2 and the largest is about 16.7 nm at 40 mW/cm^2. This variation is because of the fact that AuNP materialization can be contingent on the morphology of PSi. The nanocrystallite size was assessed from the peak width as exposed in Fig. 6(a–d), and it can be attained by Scherer's formula as follows [6]:

The specific surface area (S.S.A) is unique of the facts of the importance of the material and known as follows [6]:

$$S.S.A = \frac{6000}{L \times \rho} \qquad (3)$$

where S.S.A is the specific surface area, L is the grain size of the AuNPs, and ρ is the density of gold (19.30 g/cm^3). The highest value of S.S.A is around 164 nm and the minimum value is about 18 nm for laser power densities 80 mW/cm^2 and 40 mW/cm^2, respectively.

Electrical Properties AuNP/PSi Hetro Structures

Figures 7, 8, and 9 illustrate the J-V characteristics of Al/PSi/n-Si/Al structures and Al/AuNP/PSi/n-Si/Al sandwich as a function to power density of 20, 40, 60, and 80 mW/cm^2 at room temperature respectively. All results were measured in the applied voltage range from 0 to 5 V in dark situation. In Figs. 7 and 8, the curves typical have Ohmic contact behavior for all porous silicon samples.
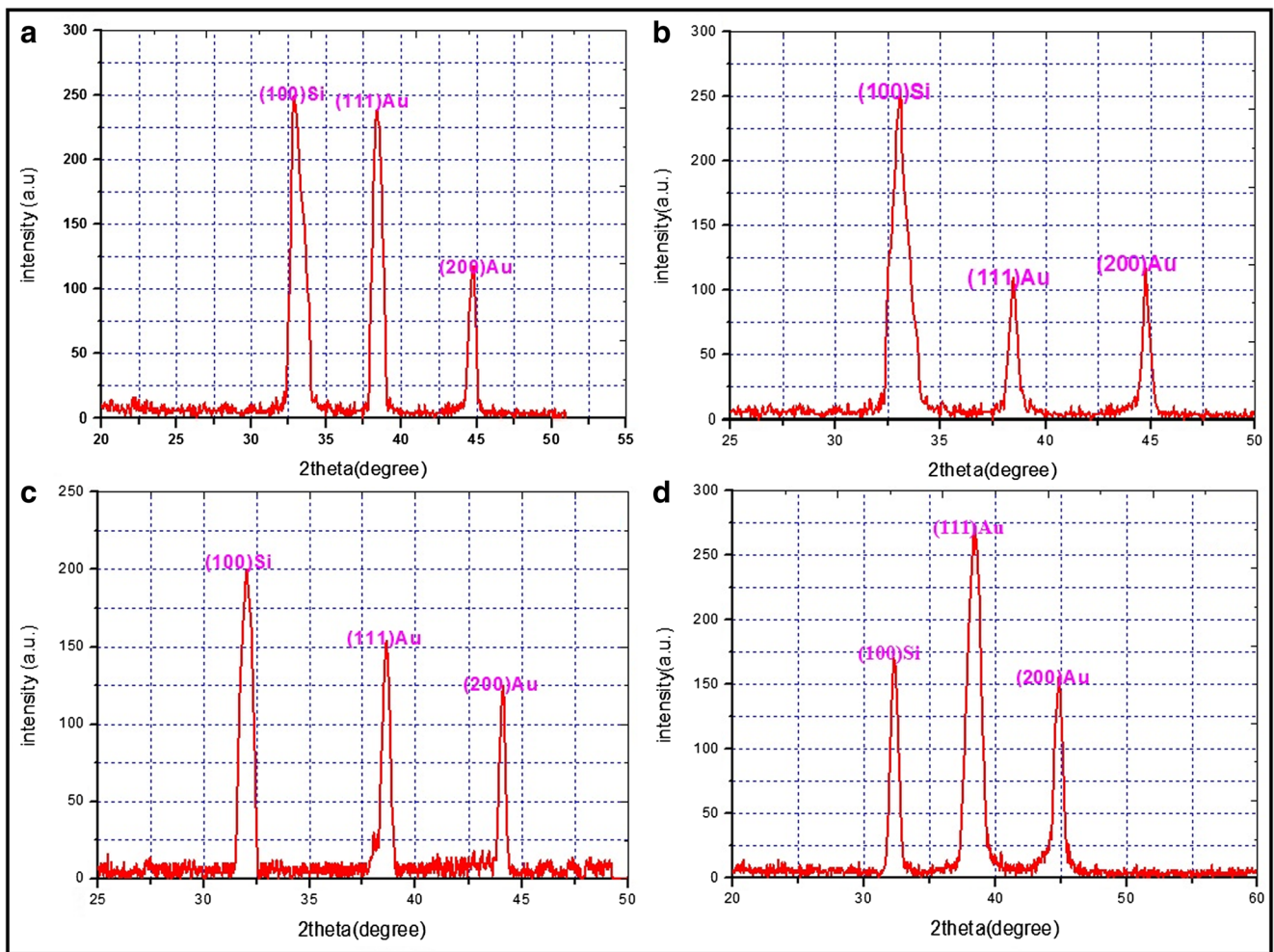
Fig. 6 XRD spectra of AuNPs as a function to laser power density: (a) 20 mW/cm^2, (b) 40 mW/cm^2, (c) 60 mW/cm^2, and (d) 80 mW/cm^2

In Fig. 8, for both curves, exposure to CO gas did not altered the form of J-V (quiet Ohmic contact) but the current at existence of CO gas was greater than that of the situation without gas, the difference in the current signifying that the sensor was SO sensitive to CO gas.

Figure 9 displays the current–voltage characteristics of the made-up gas sensors of AL thin/AuNP/PSi/n-Si/AL

electrode), the forward current–voltage performance as Schottky junction [10]. The rising of the current in the presence of CO gas caused by adsorbate interaction with PSi dangling bond is essentially associated to enhancement of the conductance differences attributable to the trapping or release of the carriers [11]. Also, the PSi surface incorporating through AuNPs improved the integrated specific surface area

Table 1 Experimental and standard X-ray diffraction angles of gold nanoparticles at different laser power densities

Laser power density (mW/cm^2)	HAuCl$_4$/HF concentration	2θ in degree at the plane (100) Experimental	2θ in degree at the plane (111) (standard = 38.100°) Experimental	2θ in degree at the plane (200) (standard = 44.369°) Experimental
20	10^{-2} M/2.8 HF	32.85	38.4	44.8
40	10^{-2} M/2.8 HF	33.1	38.45	44.75
60	10^{-2} M/2.8 HF	32.02	38.64	44.1
80	10^{-2} M/2.8 HF	32.3	38.41	44.81

Table 2 Grain size of the AuNPs in planes (111) and (200)

Laser power density (mW/cm^2)	HAuCl$_4$/HF concentration	Plane (111)			Plane (200)		
		FWHM (rad)	Grain size of AuNPs (nm)	S.S.A of AuNPs (m^2/g)	FWHM (rad)	Grain size of AuNPs (nm)	S.S.A of AuNPs (m^2/g)
20	10^{-2} M/2.8 HF	0.019	8.8	35	0.017	10	31
40	10^{-2} M/2.8 HF	0.01	16.7	18	0.014	12	26
60	10^{-2} M/2.8 HF	0.02	8	39	0.015	11	28.3
80	10^{-2} M/2.8 HF	0.88	1.9	164	0.059	3	104

of the porous silicon/gold nanoparticle structure and henceforth increased the gas adsorption rate. The current response of the sensor (sensitivity) S% is assessed by Eq. (4) in terms of current instead of the resistance due to the fact that the device is operated in sandwich form rather than the planar form:

$$S = \left| \frac{I_{gas} - I_{air}}{I_{air}} \right| \qquad (4)$$

where I_{gas} and I_{air} characterize the current in the presence and absence of CO gas respectively [6, 10]. The successive current responses with time when CO gas at a pressure of 2 mbar. For sensors, AL thin/AuNP/PSi/n-Si/AL electrode structure gas sensor and as-formed PSi substrates without of incorporation of gold nanoparticles, both adsorption and desorption times were set 4 min. Fresh air flowed in the cavity. The response time is well known as the time required for the sensor to reach 0.9 of maximum current from early value while the recovery time is well defined as the time taken from maximum current to reach 0.1 of its maximum current value [12]. From the figure, both response and recovery times were less for AL thin/AuNP/PSi/n-Si/AL electrode sensor compared with as-formed PSi substrate sensor.

From Figs. 7 and 8, the maximum variation was obtained at laser power density 80 mW/cm^2 due to the complex forms of pores (double structure), and this will improve the gas adsorption process between the molecules and the porous matrix.

Figure 9 shows the current responses of prepared sensors are done by the double structure better than meso and macro structures at existence CO gas. This means that the fabricated sensor was very sensitive to morphological properties of the double porous layer the increasing the etching time would be increased the specific area (active sensitivity area) and also at adding Au nanoparticles increased the specific surface area and sensitivity. The increasing of the current density for all samples related to the role of the CO molecules where adsorption of the molecule on the porous silicon layer was due to the Van der Waals interaction which would lead to modifying the dielectric constant of the porous layer, whereas the presence of the CO gas would enhance the current flow in the fabricated sensor. According to the CO molecules that acted as acceptor, this would lead to an increase in the free carrier concentration. This causes a rapid increase in the passing charge carriers and hence an increase in the sensitivity.
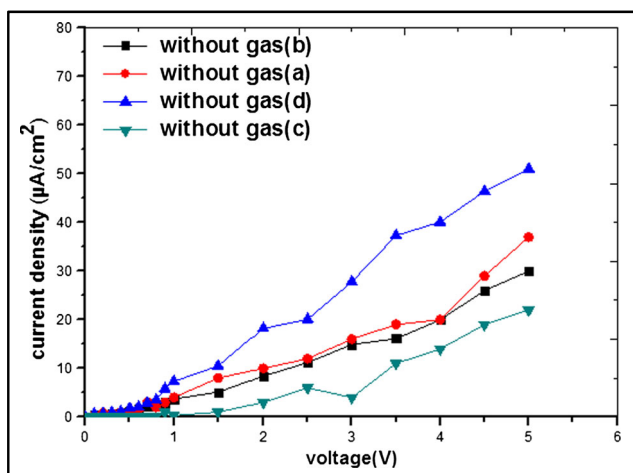

Fig 7 J-V characteristic of Al/PSi/n-Si/Al prepared without gas as a function to laser power density: (a) 20 mW/cm^2, (b) 40 mW/cm^2, (c) 60 mW/cm^2, and (d) 80 mW/cm^2
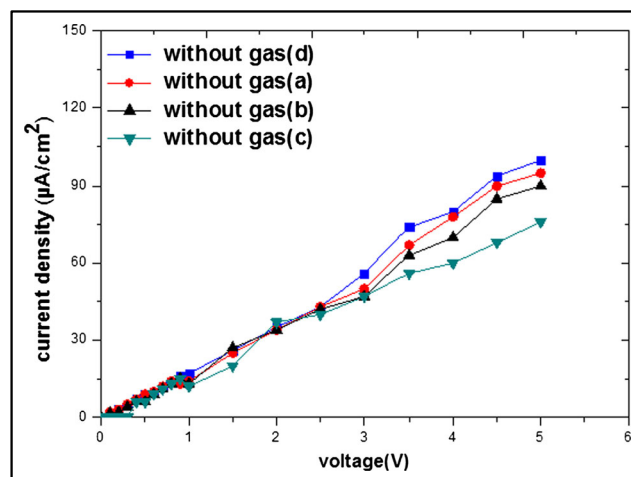

Fig 8 J-V characteristic of Al/PSi/n-Si/Al prepared with 2-mbar gas pressure as a function to laser power density: (a) 20 mW/cm^2, (b) 40 mW/cm^2, (c) 60 mW/cm^2, and (d) 80 mW/cm^2
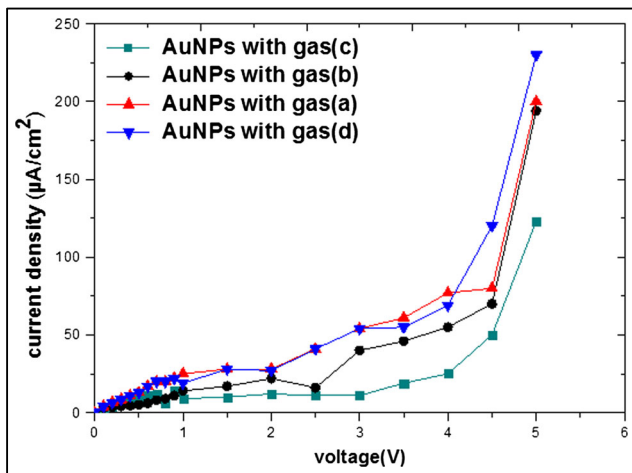
Fig. 9 J-V characteristic of Al/AuNP/PSi/n. with 2-mbar gas pressure as a function to laser power density: (a) 20 mW/cm^2, (b) 40 mW/cm^2, (c) 60 mW/cm^2, and (d) 80 mW/cm^2

Conclusion

A porous silicon (PSi)/gold nanoparticle (AuNP) hetro structures have been used to detect low CO gas pressure employing three different forms of PSi morphology: meso, macro, and double layers. The roles of increasing laser illumination power density on the morphology of n-PSi wafer displayed an opportunity to synthesize different PSi morphologies with different pore forms and sizes. The morphology of AuNPs and its size distributions were entirely dependent on PSi morphology. AuNP growth centers were mainly concentrated on the pore walls. Based on the J-V characteristics in primary vacuum and with CO, the sensitivity showed that PSi surface morphologies strongly influenced the sensor performance. The lower AuNP sizes could be occasioned in high and fast current response.

References

1. Canham LT (1990) Silicon quantum wire array fabrication by electrochemical and chemical dissolution of wafers. Appl Phys Lett 57:1046–1048
2. Jawad MJ, Hammod HY, Dheyab AB (2015) Effect of thermal annealing temperatures on MSM Photo detector based on Ge-like micro flowers in the dark mode. J Electr Eng 16(3):502–508
3. Yamazoe N, Shimanoe K (2009) Receptor function of small semiconductor crystals with clean and electron-traps dispersed surfaces. Thin Solid Films 517:6148–6155
4. Alwan AM, Abbas RA (2017) Effects of the porous silicon morphology on the gas sensor performance. IJESRT 6(1): January, IC™ Value: 3
5. Bisi O, Ossicini S, Pavesi L (2000) Porous silicon: a quantum sponge structure for silicon based optoelectronic. Surf Sci Rep 38(1–3):1–126
6. Azraf M (2013) Formation of porous silicon application [Master's Thesis]. Johor (MY): Universiti Teknologi Malaysia; 63 pp
7. Liua X, Wang A, Li L, Zhang T, Moub C-Y, Leec J-F (2013) Synthesis of Au–Ag alloy nanoparticles supported on silica gel via galvanic replacement reaction. Materials International 23(3): 317–325
8. Alwan AM, Dheyab AB (2017) Room temperature CO2 gas sensors of AuNPs/mesoPSi hybrid structures. Appl Nanosci:7–335
9. Alwan AM, Dheyab AB, Allaa AJ (2017) Study of the influence of incorporation of gold nanoparticles on the modified porous silicon sensor for petroleum gas detection. J Eng And Technology, University of Technology, Part A, No 8, 35
10. Alwan AM, Abbas RA, Dheyab AB (2018) Study the characteristic of planer and sandwich PSi gas sensor (comparative study). Silicon, Issue 2
11. Alwan M. Alwan, Rasha B. Rashid, Amer B. Dheyab (2018) Morphological and electrical properties of gold nanoparticles/macro porous silicon for CO2 gas., Vol. 59, No.1A, pp: 57–66
12. Gole J, Ozdemir S ((2009)) Metal coating of porous silicon gas sensors for improved sensitivity & selectivity. Thomas Osburn, Georgia Tech Physics, MSE SURF Fellow